Preprints of the 19th World Congress
The International Federation of Automatic Control
Cape Town, South Africa. August 24-29, 2014

Declutching Control of Wave Energy Converters using Derivative-Free Optimization

Zhe Feng * **Eric C. Kerrigan** **

* *Department of Electrical & Electronic Engineering, Imperial College London, London, SW7 2AZ, UK (e-mail: zhe.feng09@imperial.ac.uk)*
** *Department of Electrical & Electronic Engineering and Department of Aeronautics, Imperial College London, London, SW7 2AZ, UK (e-mail: e.kerrigan@imperial.ac.uk)*

Abstract:
We propose a novel formulation for declutching control of wave energy converters with the power take-off time as the only decision variable. The optimal control problem is modeled as a single-variable optimization problem, thereby making real-time implementation a possibility. We present a derivate-free optimization algorithm that exploits the quantization of the decision variable in order to reduce the number of function evaluations needed to compute a solution. We propose two receding horizon closed-loop strategies: the first one uses past wave information and can increase the energy generation by 42% compared to the uncontrolled case, while the second formulation uses predictions of future waves and results in a further 40% increase in energy generation. For irregular waves with peak periods longer than 6 s, one can generate at least four times more energy when co-designing the physical system and controller, compared to a controlled system that was optimized without a controller in the feedback loop.
Key Words: derivative-free optimization, declutching control, wave energy, coordinate-search

1. INTRODUCTION

The energy absorption of wave energy converters (WECs) can be significantly improved by various control strategies, as suggested by Falnes [2007], Budar [1975] and Abraham and Kerrigan [2013a]. This paper will study a control implementation for WECs known as declutching control. Declutching control can increase the power take-off (PTO) of WECs in a wide frequency range, particularly for devices whose resonant period is longer than the incident wave's peak period. Declutching control works by bypassing the PTO mechanism for certain time intervals, thereby effectively altering the resonant frequency of the device to match the frequency of the incident wave. Detailed physical implementations can be found in Babarit et al. [2009] and Clément and Babarit [2012]. Declutching control is passive, easy to implement and more importantly, does not have violent cut-off actions as with latching control. Hence, declutching control is of great interest to many practitioners [Falnes, 2001, Salter, 1979]. Furthermore, designing an algorithm for controlling a two-mode system provides control theoreticians with an interesting example problem.

In this paper, we will modify the latching control algorithm in Feng and Kerrigan [2013], which is based on derivative-free optimization (DFO), to declutching control. Unlike latching control, for declutching control the cost function is continuous in most cases. However, the analytical gradient is very hard to obtain and a finite difference method will struggle due to the fact that the decision variable is quantized (this will be discussed in Section 2.2). Thus, reliable performance of derivative-based optimization methods is not guaranteed. Furthermore, since we have a univariate cost function, the computational cost of derivative-free optimization methods is low. Two formulations will be studied: a past data formulation, which uses recorded past wave data, and a future data formulation, which requires the prediction of future waves.

The paper is organized as follows: in Section 2 a declutching controlled WEC model will be described and we will demonstrate some properties of the cost function. In Section 3 we will briefly introduce the coordinate-search optimization method. We will discuss two closed-loop problem formulations in Section 4. Section 5 will present some simulation results, where we will demonstrate the benefit of cyber-physical co-design of the WEC, as well as compare our optimization method against other algorithms for univariate optimization. Finally, we will end with conclusions and suggestions for future work.

2. MODEL AND PROBLEM FORMULATION

2.1 Model of Wave Energy Converter

The model of a WEC used here is based on linear wave theory, due to its simplicity and sufficient accuracy for control applications. In the time domain, the model is given by:

$$(M+\mu_\infty)\ddot{\zeta}(t)+\int_0^t K(t-\tau)\dot{\zeta}(\tau)d\tau+B_{pto}\dot{\zeta}(t) + (k_s+\rho g S)\zeta(t)=F_e(t), \quad (1)$$

where ζ is the displacement of the WEC buoy from the equilibrium, M is the mass of the buoy, μ_∞ is the infinite frequency added mass, $K(\cdot)$ is the impulse response kernel, B_{pto} and k_s are the PTO damping coefficient and the spring constant of the PTO mechanism, respectively, ρ is the water density, g is the gravity constant, S is the submerged cross-section area of the buoy and $F_e(\cdot)$ is the excitation force caused by incident waves. The model (1) is widely used in WEC control studies, for example in Babarit and Clément [2006] and Clément and Babarit [2012].

The system (1) is a differential-integral equation. The integral term causes difficulty in analysis and can be simplified, as suggested in Yu [1995], Loan [1978] and Kristiansen [2005]. The integral $B_{rad}(t) := \int_0^t K(t-\tau)\dot{\zeta}(\tau)d\tau$ can be approximated as the output of a state-space system:

$$\dot{q}(t) = A_r q(t) + B_r \dot{\zeta}(t), \tag{2a}$$
$$B_{rad}(t) = C_r q(t) + D_r \dot{\zeta}(t), \tag{2b}$$

with an approximation order of n_r, where $q(t) \in \mathbb{R}^{n_r}$ is the approximation state, and A_r, B_r, C_r, D_r are the coefficient matrices of the approximating system. These coefficient matrices are calculated via the impulse to state-space technique proposed in Kristiansen [2005].

According to Babarit et al. [2009], if we activate the PTO mechanism when $v(t) \neq 0$, the system may undergo high stresses. On the other hand, in simulation results, the optimal time instance for activating the PTO mechanism is mostly at $v(t) = 0$ [Abraham and Kerrigan, 2013a, Babarit et al., 2009]. It is clear that $v(t) = 0$ is often the best practical switching point for the PTO mechanism. Therefore, we propose a sub-optimal declutching control scheme that is similar to latching control: we activate the PTO mechanism whenever $v(t) = 0$ and declutch the PTO mechanism after t_a seconds.

The dynamics of such a declutching-controlled system can be described as a hybrid system in terms of a timed automaton [Lee and Seshia, 2011, Chap. 4]. We assume that when the system is declutched, the damping B_{pto} becomes zero, i.e. no energy is generated in the declutched mode. Figure 1 shows the timed automaton representation of the declutching-controlled system, where $v(\cdot) := \dot{\zeta}(\cdot)$ is the velocity of the buoy. First, define a clock with dynamics $\dot{\Xi}(t) = 1$ and let $z(t) := \left[\zeta(t)\ v(t)\ q^T(t)\right]^T$ be the state of the system. Let the dynamics of the two different modes be:

$$g_1(z, F_e; t) := \begin{bmatrix} v(t) \\ \frac{1}{M_T}[-k_T\zeta(t) - D_r v(t) - C_r q(t) \\ \qquad + F_e(t)] \\ A_r q(t) + B_r v(t) \end{bmatrix}, \tag{3a}$$

$$g_2(z, F_e; t) := \begin{bmatrix} v(t) \\ \frac{1}{M_T}[-k_T\zeta(t) - (B_{pto} + D_r) v(t) \\ \qquad - C_r q(t) + F_e(t)] \\ A_r q(t) + B_r v(t) \end{bmatrix}, \tag{3b}$$

where $M_T := M + \mu_\infty$ and $k_T := (k_s + \rho g S)$. g_1 describes the dynamics in the declutched mode. The resonant period in this mode is slightly shorter than the PTO-active mode. g_2 describes the PTO-active mode, i.e. when the system's PTO damping B_{pto} is engaged and the power is generated. Whenever the velocity $v(t) = 0$, the clock is reset $\Xi(t) := 0$, the system transits from the declutched mode to the PTO-active mode and stays in this mode for t_a seconds. The time during which the system is in the PTO-active mode is termed the PTO-active time.

We assume full state feedback. However, a state estimator can be constructed by modelling the WEC as a linear time-varying system, where B_{pto} is a known function of time. Alternatively, one can model the system as a linear differential inclusion and follow the same procedure outlined in Abraham and Kerrigan [2013b].

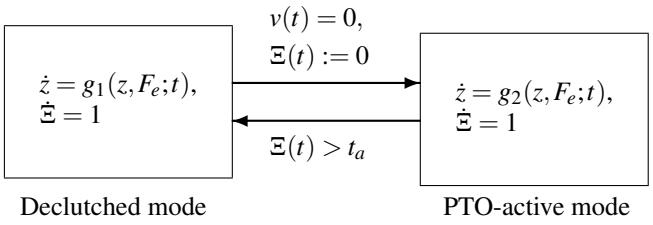

Fig. 1. Declutching-controlled WEC system.

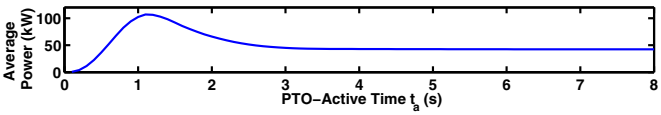

Fig. 2. Average power generated against t_a under an irregular wave with park period 7 s for a 2000 s simulation.

2.2 Cost Function and the Optimization Problem

With a given WEC system, one aims to maximize the energy absorption over a time horizon, say from $t = a$ to $t = b$. The power extracted by the system depends on the damping coefficient of the PTO mechanism and the velocity of the buoy, i.e. $\hat{B}_{pto}(t; t_a)v^2(t)$, where $\hat{B}_{pto}(t) = B_{pto}$ if the system is in the g_2 mode and $\hat{B}_{pto}(t) = 0$ if the system is in the g_1 mode.

In declutching control, the optimal control problem over a horizon starting at $t = a$ and ending at $t = b$ can be defined as:

$$\max_{t_a \geq 0} J(z_a, t_a, F_e, a, b) := \int_a^b \hat{B}_{pto}(t) v^2(t; z_a, t_a, F_e|_{[a,b]})dt, \tag{4}$$

where $J : \mathbb{R}^n \times \mathbb{R}_+ \times \mathscr{L}^p \times \mathbb{R} \times \mathbb{R} \to \mathbb{R}_+$ depends on the initial state $z_a := z(a)$, control variable t_a and $F_e|_{[a,b]} : [a,b] \to \mathbb{R}$, the excitation force function over the integration interval.

Figure 2 shows the energy absorption against t_a when the WEC described in Section 5 is subjected to a Joint North Sea Wave Project (JONSWAP) spectrum-generated excitation force with a peak period of 7s. Such an excitation force is often used to simulate irregular wave conditions [Babarit and Clément, 2006]. Unlike the discontinuous cost function for latching control observed in Feng and Kerrigan [2013], the cost function of declutching control appears to be continuous. However, note that this is not always the case: the function can be discontinuous, as we will show later.

We will first provide a condition when the cost function is continuous. Consider that the declutching-controlled system (3), which can be written as:

$$\dot{z}(t) = A_0 z(t) + B F_e(t),\ \forall t \in [t_0,\ t_1) \cup [t_i + t_a,\ t_{i+1}), \tag{5a}$$
$$\dot{z}(t) = A_1 z(t) + B F_e(t),\ \forall t \in [t_i,\ t_i + t_a), \tag{5b}$$

where t_i, $i = 1, \ldots, N_v$, are the N_v zero-crossing points of $v(t)$ over a time horizon and $v(t)$ is the second element in the state $z(t)$. A_0, A_1 and B are the coefficient matrices.

The two solutions of the linear sub-systems (5a) and (5b) are:

$$\Phi_0(z(a), a, b) = e^{A_0(b-a)}z(a) + \int_a^b e^{A_0(b-\tau)} B F_e(\tau)d\tau,$$
$$\Phi_1(z(a), a, b) = e^{A_1(b-a)}z(a) + \int_a^b e^{A_1(b-\tau)} B F_e(\tau)d\tau.$$

Without loss of generality, assume the system starts in mode (5b), then the solution of system (5) is given by

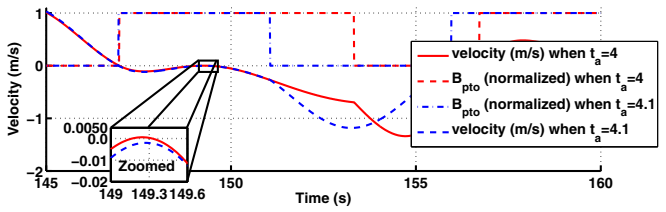

(a)

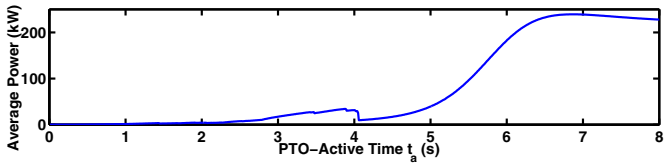

(b)

Fig. 3. (a) Simulation showing that, when t_a changes from 4 s to 4.1 s, the zero-crossing point at $t = 149.3$ s vanishes. (b) The cost function for a sinusoidal excitation force of period 18 s; the function is discontinuous at $t_a = 4$ s.

$$z(t;t_a) = \Phi_0(\Phi_1(\Phi_0(\Phi_1(\cdots\Phi_0(z_0,0,t_1),\cdots,t_{n-1}+t_a,t), \forall t \in [t_{N_v-1}+t_a,\ t_{N_v}). \quad (6)$$

If $F_e(\cdot)$ is continuous, then $\phi_0(\cdot)$ and $\phi_1(\cdot)$ are continuous. As a result, if the number of the function compositions does not change, then the composite function (6) will be continuous in t_a and, consequently, the cost function in (4) will be continuous in t_a.

For the declutching controlled system (3), there is no violent cut-off actions as in latching control. The system is controlled by bypassing the PTO machinery; hence, the number of zero-crossing-points seldom change and the cost function is continuous in most cases. However, even for sinusoidal waves, if the period of the incoming wave is significantly longer (or shorter) than the resonance period of the device, it is possible that the number of zero-crossing points will change. Consequently, the number of compositions in (6) will change and it is possible that the trajectory $z(\cdot;t_a)$ will have a discontinuity for some t_a. Such a situation is shown in Figure 3(a): when $t_a = 4$ s, the velocity at $t = 149.3$ s has two zero-crossing points very close to each other and the PTO-active time is thus extended by 4 s after $t = 149.3$ s. However, any increase in t_a will result in the two zero-crossing points reducing to a zero-touching point. This is shown in Figure 3(a) when $t_a = 4.1$ s; since the zero-crossing-points vanished, the PTO-active time only lasts for 4 s. Note that, immediately after $t = 151$ s, the two velocity trajectories become different. Hence, following a similar analysis in Feng and Kerrigan [2013], one can conclude that discontinuities will arise in the cost function, as in Figure 3(b).

Moreover, because in applications the system is often discretized in time, t_a can only be drawn from a countable set $S_{ta} := \{t_a | t_a = jh \text{ for } j = 0,1,\cdots,j_{max}\}$, where $h > 0$ is the sampling period and $j_{max}h =: \bar{t}_a$ is the largest admissible value for the PTO-active time (which should usually be less than the peak period of the incoming wave). Therefore, we replace the problem in (4) with

$$\max_{t_a \in S_{ta}} J(z_a,t_a,F_e,a,b) := \int_a^b \hat{B}_{pto}(t)v^2(t;z_a,t_a,F_e|_{[a,b]})dt, \quad (7)$$

where the decision variable is quantized.

Algorithm 1 One-dimensional coordinate search (CS)

Require: $f(\cdot)$: objective function; x_0: initial guess; $\alpha_0 \in S_{ta}\backslash\{0\}$: initial step size; $\gamma > 1$, $\beta \in (0,1)$: step size update parameters; h: sampling time (tolerance);

Ensure: Locally optimal x^*.

Define

$$\hat{f}(x) := \begin{cases} f(x) & \text{if } x \in [0, j_{max}h] \\ -\infty & \text{if } x < 0 \text{ or } x > j_{max}h \end{cases}.$$

Set $i := 0$.

repeat

1. Poll step: Let the poll set be defined as $P_i := \{x_i + \alpha_i,\ x_i - \alpha_i\}$. If $\exists \hat{x} \in P_i$ s.t. $\hat{f}(\hat{x}) > \hat{f}(x_i)$, then set $x_{i+1} := \arg\max_{\hat{x} \in P_i} \hat{f}(\hat{x})$ and claim the poll step as successful.

2. Parameter update: If the poll step was successful, set $\alpha_{i+1} := \lceil \frac{\gamma\alpha_i}{h} \rceil h$. If the poll step was unsuccessful, set $x_{i+1} := x_i$ and $\alpha_{i+1} := \lfloor \frac{\beta\alpha_i}{h} \rfloor h$.

3. Increment i

until $\alpha_i < h$

Gradient-based optimization methods are clearly not suitable for this application. Although it seems that the cost function is smooth in most of the cases, it is possible that the cost function will be discontinuous. Moreover, even in the smooth case, the analytical derivative is hard to find. Consequently one cannot expect gradient-based methods to be numerically robust.

3. DERIVATIVE-FREE OPTIMIZATION

As discussed in Section 2.2, derivative-based optimization methods are not appropriate in this application. We choose to adapt the derivative-free coordinate search (CS) method discussed in Feng and Kerrigan [2013]. Here we only briefly present the algorithm specialized for declutching control; a detailed discussion can be found in Feng and Kerrigan [2013].

For declutching-control considered here, the generic CS algorithm becomes a simple two-directional line search procedure, which is summarized in Algorithm 1. The problem solved is

$$\max_x f(x) := \max_x J(z_0,x,F_e,a,b),$$

where the decision variable x in this case is the PTO active time t_a. Each iteration of Algorithm 1 evaluates points that are α_i away from the current iterate and compare their values. If a cost increase is detected, the current iterate is replaced by the new point and the step size is increased. Otherwise, the algorithm stays at the current point and reduces the step size in order to try and find a point with higher cost.

Note that Algorithm 1 is different from the algorithm presented in Feng and Kerrigan [2013]. In Algorithm 1, $\alpha_0 \in S_{ta}\backslash\{0\}$ means that α_0 is drawn from S_{ta} but not 0. We take $\alpha_{i+1} := \lceil \frac{\gamma\alpha_i}{h} \rceil h$ to round α_{i+1} to the nearest number in S_{ta} that is larger than $\gamma\alpha_i$; or we take $\alpha_{i+1} := \lfloor \frac{\beta\alpha_i}{h} \rfloor h$ to round α_{i+1} to the nearest number in S_{ta} that is smaller than $\beta\alpha_i$. Therefore, the sequence generated by the algorithm ensures $x_i \in S_{ta}$, so the algorithm does not evaluate points that are not feasible. The tolerance is h, which is the smallest change in t_a. By contrast, the algorithm presented in Feng and Kerrigan [2013] evaluates points in an uncountable set of reals, most of which may not be feasible and hence results in redundant function evaluations.

Algorithm 2 Closed-loop Receding Horizon Implementation

Require: Equivalent discrete-time systems $z((k+1)h) = \hat{g}_1(z(kh),F_e;k)$ and $z((k+1)h) = \hat{g}_2(z(kh),F_e;k)$; initial timer $\Xi(0) := 0$; initial PTO active time $\xi(0) := 0$; initial point for optimization solver $t_{a0} := 0$.
for each sampling instance $k = 0,1,\ldots$ **do**
  if $v((k-1)h)\cdot v(kh) \le 0$ **then**
    Compute $\xi(k) := t^*_{as}(z,F_e,kh)$, where $s \in \{p,f\}$
    Reset timer $\Xi(kh) := 0$
  end if
  if $\Xi(kh) \le \xi(k)$ and $\xi(k) > 0$ **then**
    $z((k+1)h) = \hat{g}_2(z(kh),F_e;k)$
  else
    $z((k+1)h) = \hat{g}_1(z(kh),F_e;k)$
  end if
  Increase timer $\Xi((k+1)h) := \Xi(kh) + h$
  Replace t_{a0} with $\xi(k)$
end for

4. CLOSED-LOOP IMPLEMENTATION

We define two closed-loop formulations for the CS algorithm: the past data formulation and the future data formulation. If we record past wave data and estimate the state of the system, we have a cost function (7) w.r.t. PTO-active time t_a. Using the model (3), one can apply Algorithm 1 to determine the best PTO-active time t^*_{ap} for the recorded horizon. Because the peak period of ocean waves is stable over a short interval, t^*_{ap} can be considered as a good estimate of the optimal PTO-active time [Clément and Babarit, 2012, Babarit et al., 2004]. We refer to the first formulation as the past data formulation; mathematically,

$$\mathbb{PD} : t^*_{ap}(z,F_e,t) := \arg\max_{t_a \in S_{ta}} J(z(t-T);t_a,F_e,t-T,t), \qquad (8)$$

where t is the current time and T is the horizon length.

On the other hand, if one can predict the future excitation force, then we propose a formulation based on the current state and the predicted excitation force. One can use Algorithm 1 to find the best PTO-active time t^*_{af} over the prediction horizon. We refer to this as the future data formulation; mathematically,

$$\mathbb{FD} : t^*_{af}(z,F_e,t) := \arg\max_{t_a \in S_{ta}} J(z(t);t_a,F_e,t,t+T). \qquad (9)$$

As in Figure 2, there often exists a unique global maximum close to zero. Thus, we propose 0 as the initial guess t_{a0} of the first optimization problem (at the first sampling instant). This makes it likely that the algorithm will converge to the global maximum, in practice. For both formulations, one can solve the optimization problem at each sampling instant using a warm start procedure to speed up convergence. If the algorithm has converged to the global maximum, then it is likely that at each subsequent sample instant the algorithm will converge to the global maximum.

For the closed-loop, one can solve problem (8) or (9) every h seconds and implement the solution in a receding horizon fashion, as is standard in predictive control. This procedure is detailed in Algorithm 2, where $s = p$ or $s = f$ depending on whether past or future wave data is available, respectively.

5. SIMULATION RESULTS

For the simulations, the parameters for the system (1) are $n_r := 5$, $M := 707\,\text{t}$ (ton), $\mu_\infty := 244\,\text{t}$, $g := 9.81\,\text{m/s}^2$, $\rho := 1000\,\text{kg/m}^3$, $S := 78.5\,\text{m}^2$, $k_s := 240\,\text{kN/m}$. The parameters for Algorithm 1 are $\gamma = 1.5$, $\beta = 0.5$. We set $h := 0.1\,\text{s}$ and $T := 20\,\text{s}$ which is the shortest horizon length that can achieve the best PTO and $\bar{t}_a := 10\,\text{s}$. Note that we assume that the switching can only occur at each sampling instance. Unless indicated otherwise, the future data formulation is used.

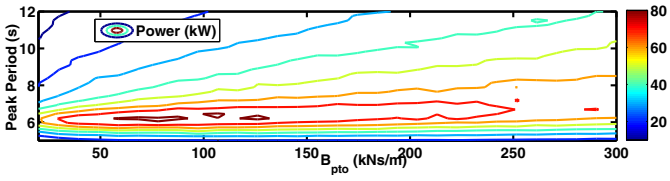

Fig. 4. PTO without control w.r.t. B_{pto} and T_p.

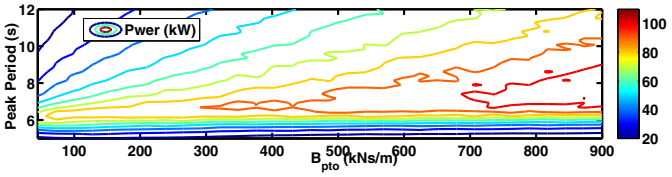

Fig. 5. PTO under declutching control w.r.t. B_{pto} and T_p.

5.1 Cyber-Physical Co-design

We briefly discuss how co-design can affect the choice of system parameters. Traditionally, the system is designed without considering the control strategy; the uncontrolled system is tuned to its optimal performance against certain working conditions. Following this, the controller is designed to maximize the system's performance. Co-design takes a different approach and designs the physical system and controller (cyber system) at the same time. In other words, the optimal physical parameters are a function of the control parameters, and vice versa.

Assume the to-be-designed parameter is the PTO damping B_{pto}. Figure 4 shows the power generated over 2000 s, subjected to irregular JONSWAP waves of peak periods T_p from 5–12 s with different values of B_{pto}. In this case, no control has been applied. Figure 4 suggests the optimal value for B_{pto} should be about 58–87 kNs/m for a significant range of periods. Thus, if we followed the standard procedure, we would take B_{pto} around 78 kNs/m. If declutching control is applied, the maximum power is about 82 kW, obtained for waves with peak periods of $T_p = 6.2\,\text{s}$.

Figure 5 shows the power take-off of the device under declutching control against B_{pto} for different wave periods. The range for B_{pto} is now increased to 1MNs/m to show the power take-off for very large B_{pto}. Figure 5 reveals that, unlike the uncontrolled case, for a declutching-controlled system, more power take-off can be achieved with a larger value of B_{pto}. Also, the peak power take-off wave period is slightly longer than for the uncontrolled case. Figure 6 shows the ratio of the power generated by the controlled system compared to the uncontrolled system. Note that there is little improvement for long peak periods. However, for short peak periods, declutching control with $B_{pto} = 900\,\text{kNs/m}$ is able to achieve at least 27% improvement, compared to an uncontrolled WEC, and a maximum of 170% improvement at about a peak period of 6 s. Therefore, after co-design we conclude that a larger B_{pto} will give a better performance under declutching control, hence we choose $B_{pto} = 900\,\text{kNs/m}$. Note that this value is 3 times

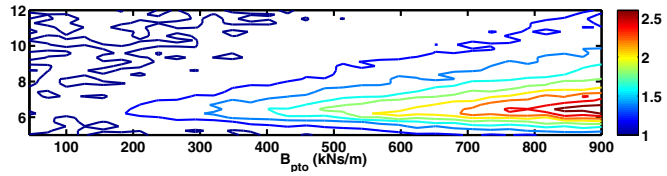

Fig. 6. Ratio of PTO with declutching control to PTO without control w.r.t. B_{pto} and T_p.

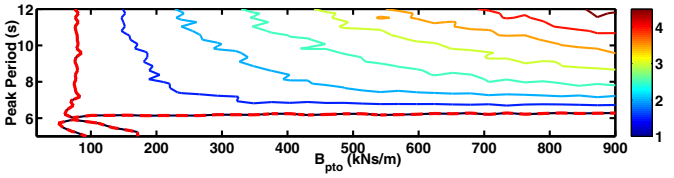

Fig. 7. Ratio of PTO with control for different T_p and B_{pto} to PTO with control for different T_p, but fixing $B_{pto} = 78$ kNs/m. The red dotted line shows where the ratio is 1.

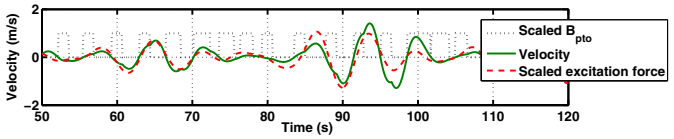

Fig. 8. Time domain simulation of future data formulation over 70 s. The incident wave height is $H_s = 2$ m and peak period $T_p = 8$ s (past data formulation is similar).

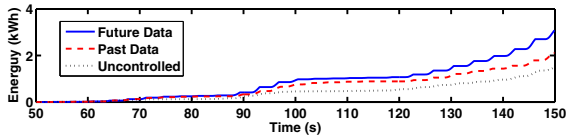

Fig. 9. Accumulative energy absorption over 100 s for both formulations with wave peak period $T_p = 6$ s.

larger than the value in Feng and Kerrigan [2013]; this is still a realistic value, since it can be achieved by large WEC devices, such as SEAREV [Babarit et al., 2009].

Figure 7 quantifies the benefits of co-design, compared to first optimizing the system without any control. Figure 7 shows the ratio of the power in Figure 5 to the power at the same peak period, but with $B_{pto} = 78$ kNs/m, as obtained above from Figure 4. For waves with $T_p < 6.2$ s, the controlled system with $B_{pto} = 78$ kNs/m performs better. However, normally WECs operate in environments with $T_p > 6$ s [Babarit and Clément, 2006]. For incident waves that have longer peak periods, note that as B_{pto} increases, the PTO ratio increases and achieves a maximum of 4.5 at $B_{pto} = 900$kNs/m with $T_p = 11$ s.

5.2 Comparison Between Past and Future Data Formulations

To test the performance of the CS algorithm for both the $\mathbb{PD}$ and $\mathbb{FD}$ formulations, the system is subjected to an irregular wave generated from a JONSWAP spectrum with a peak period of 8 s. The time domain simulation results are shown in Figure 8 for $B_{pto} = 900$ kNs/m. Figure 9 shows the accumulated energy absorption, where it can be seen that the $\mathbb{PD}$ formulation results in about 42% more energy generated than for the uncontrolled case. The $\mathbb{FD}$ formulation results in another 40% increase over the $\mathbb{PD}$ formulation.

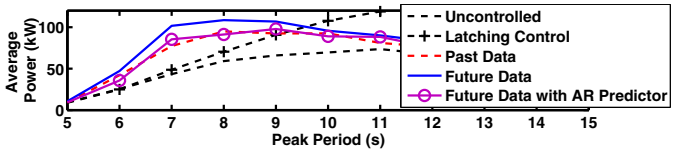

Fig. 10. Comparison of PTO for different incoming wave peak periods over 2000 s.

Figure 10 shows the average power take-off of declutching control for different wave peak periods. As Figure 10 reveals, if the wave peak period T_p is shorter than the resonant period of the system (in this case at about $T_p = 11$ s), the power take-off is significantly increased with control, for both the past-data and future-data formulations. Observe also that the maximum is shifted from $T_p = 11$ s to about 7 or 8 s.

The crossed line in Figure 10 shows the power take-off of the same WEC under the latching control of Feng and Kerrigan [2013]. Clearly, for short incoming wave periods declutching control outperformed latching control. However, for longer incoming wave periods latching control is more advantageous.

The circle-dash-dot line in Figure 10 shows the future data formulation with an auto-regression (AR) model for predicting the future incoming wave [Fusco and Ringwood, 2010]. The window length (order) of the AR predictor is 100 samples, the prediction horizon 20 s and the past data length used to train the AR predictor is 50 s. The prediction was considered to be sufficiently accurate up to $4 - -5$ s into the future. Note that the future data formulation with AR predictor has a similar performance compared to using past data, despite relatively inaccurate predictions beyond 5 s.

5.3 Comparison with Other Univariate Optimization Methods

Algorithm 1 was compared against four other methods, namely gradient ascent, golden section search, simulated annealing and exhaustive search, in terms of the number of function evaluations. At each sampling time, we solved the $\mathbb{FD}$ problem. The results for Algorithm 1, which took an average of 7 function evaluations per problem, with a maximum of 26 and a minimum of 6, are shown in Figure 11(a).

Gradient Ascent A gradient ascent method, along with a backtracking line search [Nocedal and Wright, 1999, Chap. 3], was tested. The gradient was calculated through a central difference method with step size of 0.2 (different step sizes were tried, but the results were similar). The gradient ascent method often got trapped in the flat region, as in Figure 2.

Golden Section Search The golden section (GS) search proceeds by repeatedly comparing and cutting the feasible interval into subsections according to the golden ratio (in order to ensure a constant convergence rate), until the termination tolerance is met. The golden section search guarantees the convergence to a local saddle point [Gill et al., 1986, Chap. 4.1.2]. The GS search took 11 function evaluations for all problems, because the golden ratio ensures a constant convergence rate. However, because one cannot choose an initial guess for the golden-section search algorithm, the GS search was often trapped in the flat region, as in Figure 2.

Simulated Annealing Simulated annealing (SA) is a widely-used global optimization method and does not require any

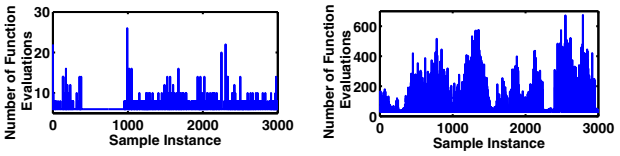

(a) Number of Function Evaluations for Algorithm 1

(b) Number of Function Evaluations for Simulated Annealing

Fig. 11. Number of function evaluations taken by different optimization algorithms for 300 s simulation with a JONSWAP wave and 0.1s sampling period

derivative information [Bertsimas and Tsitsiklis, 1993, van Laarhoven and Aarts, 1987]. Analogous to physical annealing processes, which are stochastic in nature, SA has the chance to converge to the global maximum. However, the rate of convergence is relatively slow. As shown in Figure 11(b), the number of function evaluations for the SA algorithm is varies from about 30 to 700 function evaluations. This is due to the probabilistic nature of the step generation. It is clear that the convergence of SA is not as fast as Algorithm 1. In fact, in many cases SA took more function evaluations than exhaustive search.

Exhaustive Search Recall that $\bar{t}_a := 10$ s and $h := 0.1$ s, hence an exhaustive search, which evaluates all points in S_{ta} and extracts the maximum, will require 100 function evaluations.

6. CONCLUSIONS AND FUTURE WORK

We proposed a control method and computationally efficient algorithm to cope with discontinuities that may arise due to the hybrid dynamics of a WEC under declutching control. An interesting feature of our method is that one need only past wave data to generate substantially more energy compared to an uncontrolled WEC. However, information of future incoming waves can also be used to further increase the energy generated.

Co-design of the physical system and controller can significantly increase the performance and robustness of a WEC, compared to the usual method of first optimizing the physical system without a controller, followed by controller design. This is because the controller significantly alters the closed-loop behaviour of a WEC, both qualitatively and quantitatively. Not only does the controller allow one to increase the power take-off for a given typical peak period, but the controller also allows one to increase the range of wave periods for which one can generate more energy, thereby extending the set of profitable operating conditions of the device. Advanced optimal control methods, coupled with co-design, could therefore become key technologies in determining the economic viability of generating power from ocean waves.

Future research could consider the PTO-active time at all of the predicted zero crossing points as independent decision variables, hence the optimization problem will no longer be univariate and more challenging to solve. It will be interesting to determine how much more power may be generated by solving this generalized problem.

ACKNOWLEDGEMENTS

Many thanks to Ming Ge for helping with the implementation of the method in Fusco and Ringwood [2010].

REFERENCES

E. Abraham and E. C. Kerrigan. Optimal active control and optimization of a wave energy converter. *IEEE Transactions on Sustainable Energy*, 4(2):324–332, 2013a.

E. Abraham and E. C. Kerrigan. Estimator design for input-constrained bilinear systems with application to wave energy conversion. In *Proc. 52nd IEEE Conference on Decision and Control*, Florence, Italy, 2013b.

A. Babarit and A. H. Clément. Optimal latching control of a wave energy device in regular and irregular waves. *Applied Ocean Research*, 28:77–91, 2006.

A. Babarit, G. Duclos, and A. H. Clément. Comparison of latching control strategies for a heaving wave energy device in random sea. *Applied Ocean Research*, 26:227–228, 2004.

A. Babarit, M. Guglielmi, and A. H. Clément. Declutching control of a wave energy converter. *Ocean Engineering*, 36 (12–13):1015–1024, 2009.

D. Bertsimas and J. Tsitsiklis. Simulated annealing. *Statistical Science*, 8(1):10–15, 1993.

K. Budar. A resonant point absorber of ocean-wave power. *Nature*, 256:185–201, August 1975.

A. H. Clément and A. Babarit. Discrete control of resonant wave energy devices. *Philosophical Transactions of the Royal Society A*, 370:288–314, August 2012.

J. Falnes. Optimum control of oscillation of wave-energy converters. In *11th International Offshore and Polar Engineering Conference*, Stavanger, Norway, June 2001. The International Society of Offshore and Polar Engineers.

J. Falnes. A review of wave-energy extraction. *Marine Structures*, 20:185–201, 2007.

Z. Feng and E. C. Kerrigan. Latching control of wave energy converters using derivative-free optimization. In *Proc. 52nd IEEE Conference on Decision and Control*, Florence, 2013.

F. Fusco and J. V. Ringwood. Short-term wave forecasting for real-time control of wave energy converters. *IEEE Transactions on Sustainable Energy*, 1(2):99–106, July 2010.

P. E. Gill, W. Murray, and M. H. Wright. *Practical Optimization*. Academic press, 1986.

E. Kristiansen. State-space representation of radiation forces in time-domain vessel models. *Ocean Engineering*, 32:2195–2216, 2005.

E. A. Lee and S. A. Seshia. *Introduction to Embedded Systems — A Cyber-Physical System Approach*. LeeSeshia.org, 1st edition, 2011.

C. F. Van Loan. Computing integrals involving the matrix exponential. *IEEE Transactions on Automatic control*, 23 (3), June 1978.

J. Nocedal and S. J. Wright. *Numerical Optimization*. Springer-Verlag New York, Inc, 1999.

S. H. Salter. Power conversion systems for ducks. In *Proc. Internat. Conf. on Future Energy Concepts*, volume 171, pages 100–108, London, September 1979. Institution of Electrical Engineers.

P. J. M. van Laarhoven and E. H. L. Aarts. *Simulated Annealing: Theory and Applications*. D. Reidel Publishing Company, 1987.

Z. Yu. State-space modelling of a vertical cylinder in heave. *Applied Ocean Research*, 17:265–215, 1995.